Supporting information

Construction of Ag nanowire @Au nanoparticles nano nests with densely stacked small gaps for actively trapping molecules to realize diversity SERS detection

Xie Tao,[a,b] Pan Li,[a,c]* Meihong Ge,[a,b] Siyu Chen,[a,b] Guangyao Huang,[a,b] Junxiang Li,[a,b] Meiting Gong,[a,b] Shirui Weng,[a,c] Liangbao Yang,[a,c]*

a. Institute of Health and Medical Technology, Hefei Institutes of Physical Science, Chinese Academy of Sciences, Hefei 230031, China.
b. University of Science & Technology of China, Anhui, Hefei 230026, China.
c. Department of Pharmacy, Hefei Cancer Hospital, Chinese Academy of Sciences, Hefei 230031, Anhui, China.

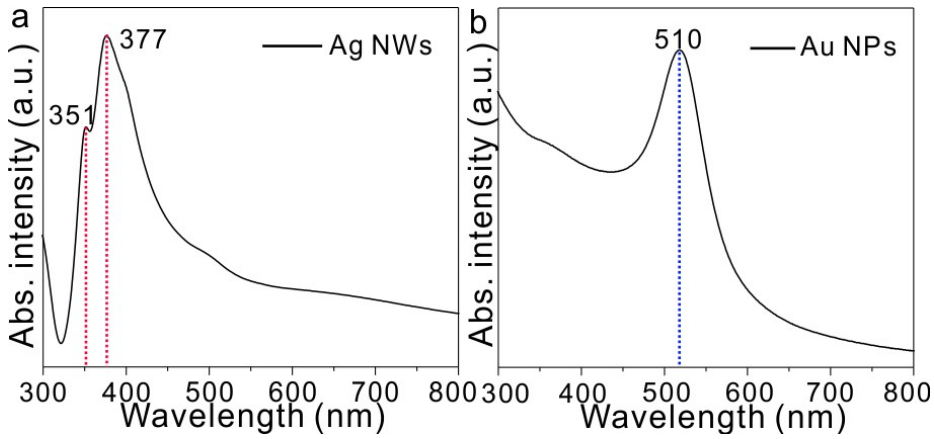

Fig. S1 UV-vis absorption of (a) Au NWs and (b) Au NPs.

The absorption peak of silver nanowires at 351 nm is due to longitudinal plasmon resonance, and the absorption peak at 377 nm is attributed to transverse plasmon resonance (Fig. S1a). The Au NPs have an absorption maximum at 510 nm (Fig. S1b).

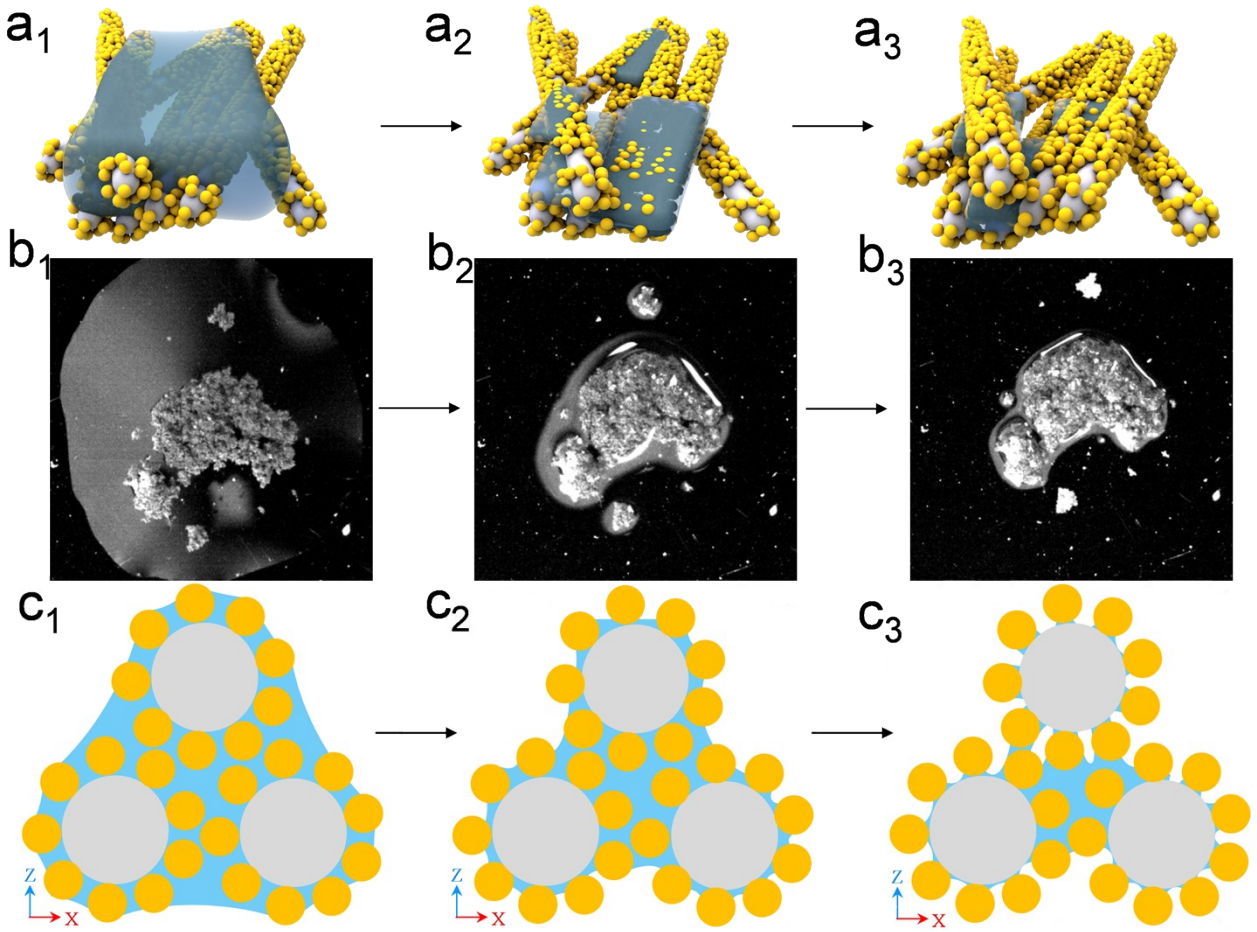

Fig. S2 Solution evaporation shrinkage process of nano-nest model (a_1-a_2); High speed photography (b_1-b_2); nano-nest model profile (c_1-c_2).

Fig. S2 shows solution evaporation shrinkage process of nano nest model (a_1-a_2); High speed photography (b_1-b_2); nano-nest model profile (c_1-c_2). In the capillary stage, the solvent shrinks from infiltration (Fig. S2a_1, $b_1$and c_1) to evaporation to form a meniscus (Fig. S2a_2, b_2 and c_2). At this time, the liquid pressure is lower than the air pressure, resulting in cohesion between the interlayer gaps. With the continuous evaporation of the solution, a liquid bridge is formed at the contact point (Fig. S2a_3, b_3 and c_3), and the molecules to be measured will further concentrate at the small gap between the layers to achieve hot spot capture of the target. [1]

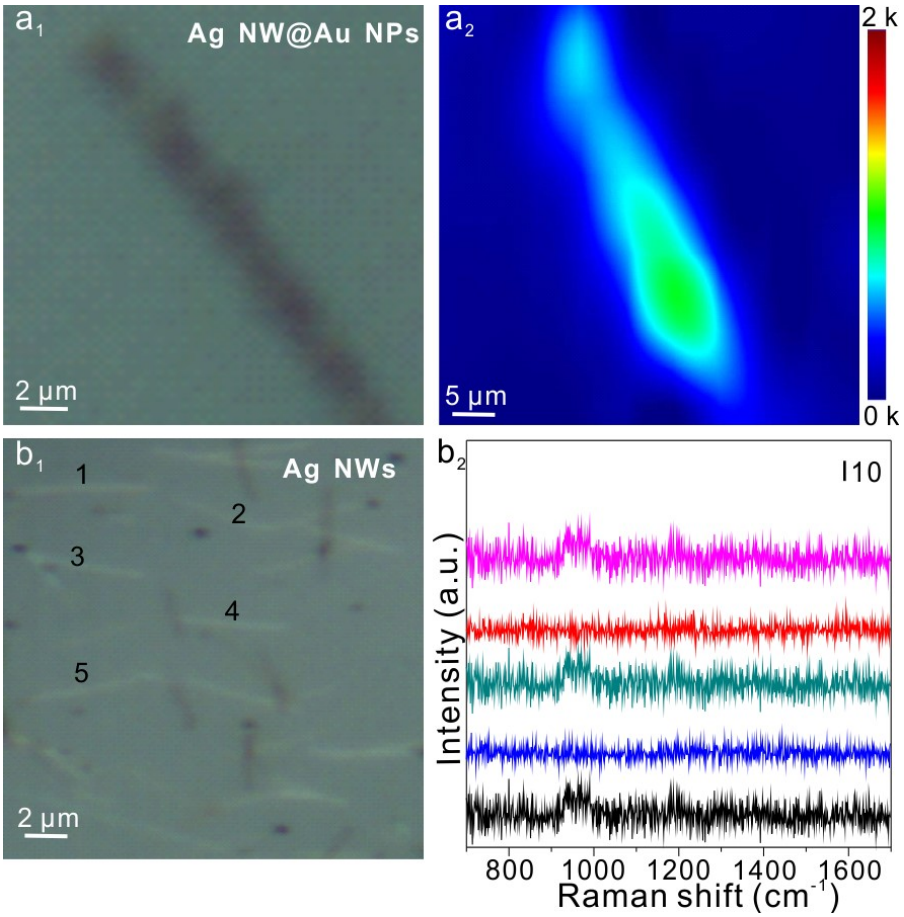

Fig. S3 Performance comparison of Ag NW @Au NPs (a) and Ag NWs (b). Raman optical microscope image and SERS mapping of Ag NW @Au NPs (a_1) and Ag NWs (b_1); SERS mapping of 10^{-7} M CV molecules at the characteristic peak 1617 cm^{-1} (a_2); SERS spectra of 10-7 M CV molecules (b_2).

Fig. S3 shows performance comparison of Ag NW @Au NPs (a) and Ag NWs (b). It can be seen that SERS performance of Ag NW @Au NPs is better than that of Ag NWs.

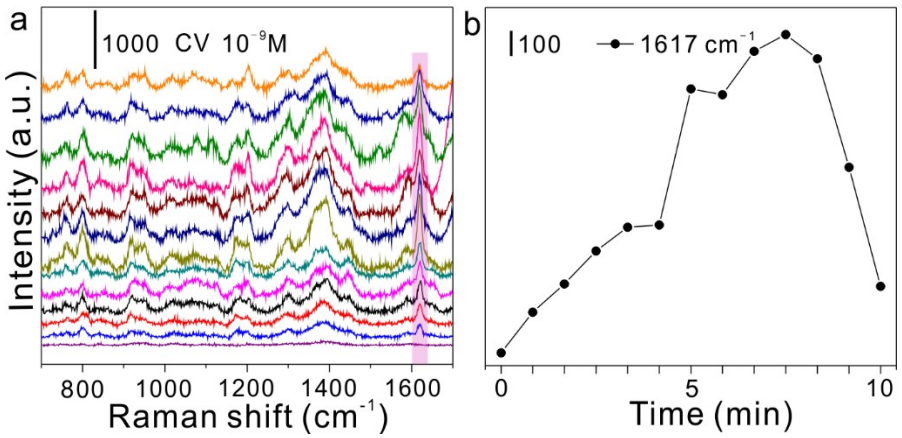

Fig. S4 (a) SERS spectra of 10^{-9} M CV solutions. (b) Time-dependent Raman spectra CV at characteristic peak 1617 cm^{-1}.

To better verify the dynamic entry of molecules into small gaps during SERS detection, we further analyzed the CV spectra as shown Fig.S4. During the dropping stage, the solution tends to flow from the large gaps of the nano nest, but not easily into the small gaps, where the signal is weaker. During the capillary stage, the solution moves through capillary action and evaporation towards densely small gaps (hot spots), where the signal starts to intensify and reaches a plateau. As the solution continues to evaporate, the molecules are not in the hot spot area and only attach to the precious metal surface, and the signal begins to weaken.

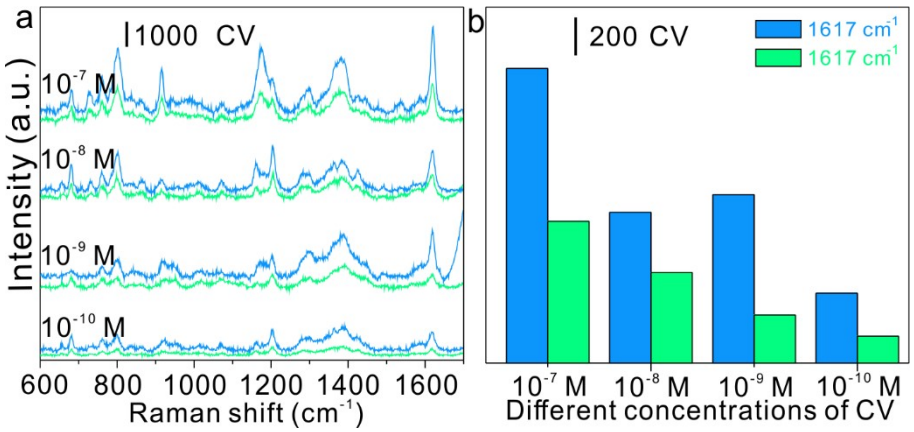

Fig. S5 Comparison of detection results between different methods (SERS spectra of CV solutions from 10^{-7} M~10^{-10} M). The blue line is the nano nest model SERS detection method, and the green line is the traditional dry state detection (a). Comparison of intensity at characteristic peak positions between different methods (b, CV at 1617 cm^{-1}).

We compared the SERS spectra of the 10^{-7} M~10^{-10} M CV solutions. The blue line is the nano nest model SERS detection method, and the green line is the traditional dry state detection in Fig. S5a. We extracted characteristic peak intensities of different methods to compare CV 1617 cm^{-1} (Fig. S5b).

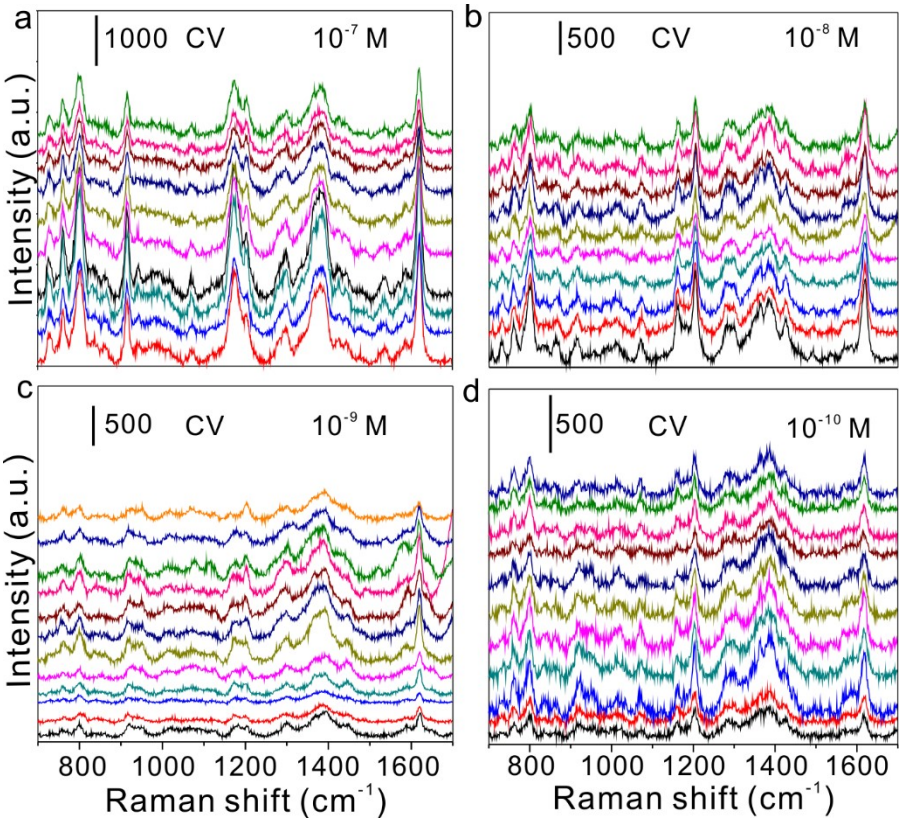

Fig. S6 SERS detection of CV by nano nest. a-d, SERS spectra of CV solutions from 10^{-7} M-10^{-10} M.

As Fig. S6 shows, we successfully realized 10^{-10} M CV detection. Characteristic peaks at 800 cm^{-1}, 1172 cm^{-1} and 1370 cm^{-1} correspond to C-H bond bending vibration, 916 cm^{-1} corresponds to ring skeleton vibration,1617 cm^{-1} corresponds to C-C stretching vibration.[2]

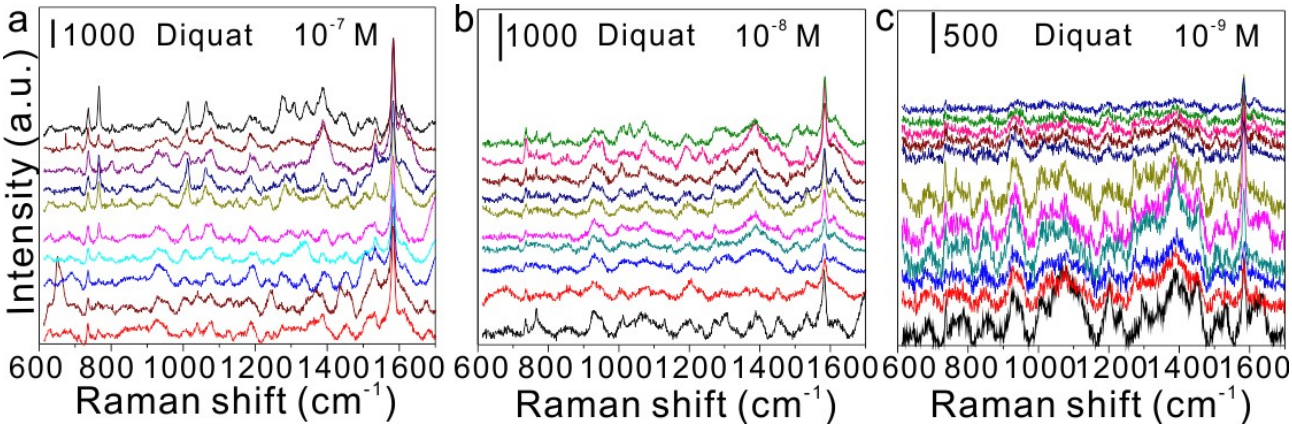

Fig. S7 SERS detection of Diquat in simulated real environment. SERS spectra of Diquat on a blade from 10^{-7} M~10^{-9} M.

Diquat is a highly toxic bipyridine herbicide, and there is no specific antidote. As Fig. S7 shows, we successfully realized 10^{-9} M Diquat detection. The characteristic peaks of Diquat are locating at 1578 cm^{-1}, 1530 cm^{-1} and 1327 cm^{-1}. The 1578 cm^{-1} and 1530 cm^{-1} are attributed to totally symmetric ring stretching vibrations, 1327 cm^{-1} can be attributed to the C-C bending vibration mode.[3]

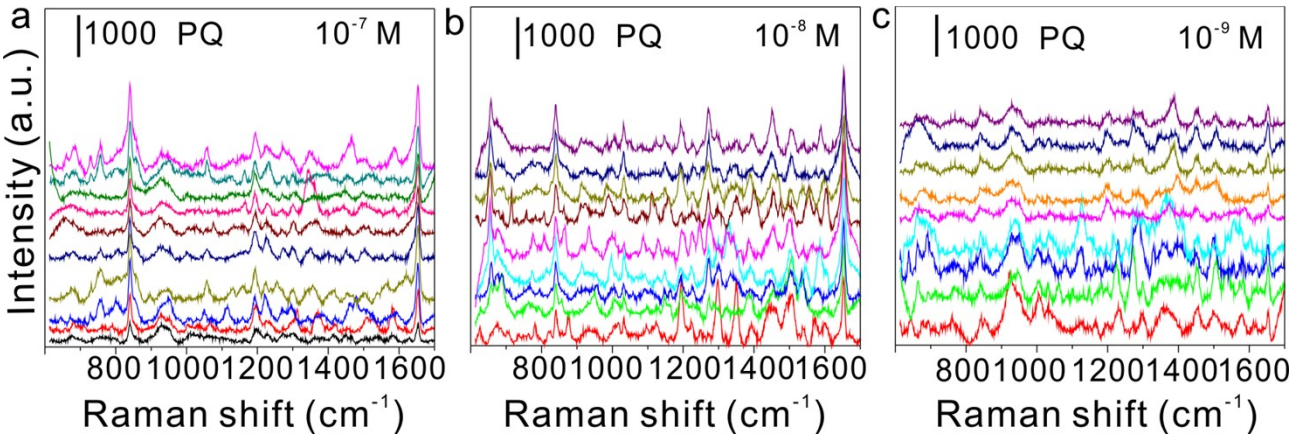

Fig. S8 SERS detection of PQ in simulated real environment. SERS spectra of PQ on a tomato from 10^{-7} M-10^{-9} M.

PQ is a widely-used and fast-acting organic heterocyclic herbicide. The exposure of it will cause great damages to the human health. The trace amount detection of PQ is urgent. As Fig. S8 shows, we successfully realized 10^{-9} M PQ detection. Four main peaks at 841 cm^{-1}, 1191 cm^{-1}, 1295 cm^{-1} and 1645 cm^{-1} correspond to four different vibration modes respectively.[4]

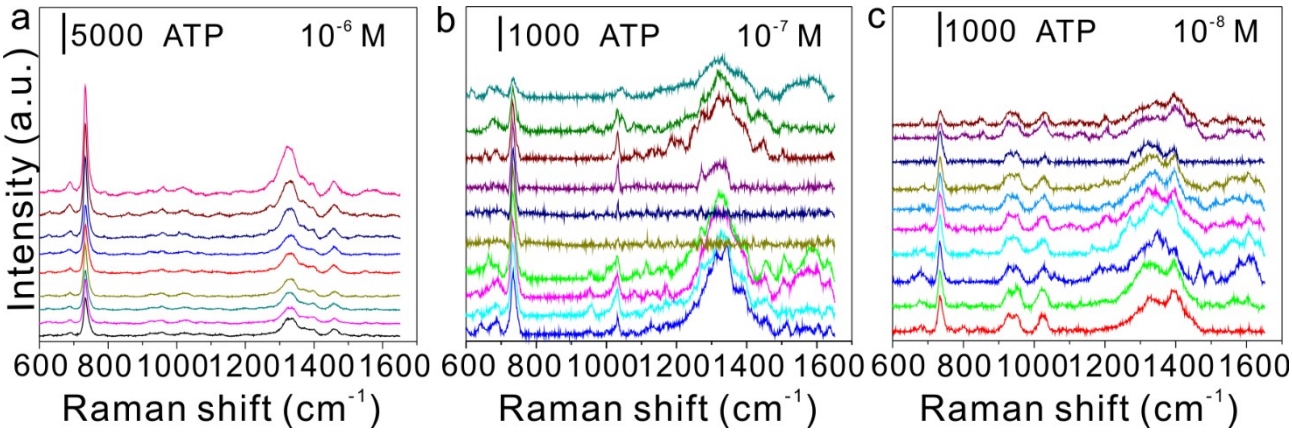

Fig. S9 SERS detection of ATP in simulated real environment. SERS spectra of ATP in cell culture medium from 10^{-6} M-10^{-8} M.

Adenosine triphosphate (ATP) plays important roles in energy storage and signaling of biological information. Most importantly, aberrant ATP levels in human fluid are strongly associated with a variety of genetic diseases. As Fig. S9 shows, we successfully realized 10^{-8} M ATP detection. Four main peaks are located at 720 cm^{-1}, 1030 cm^{-1}, 1320m^{-1} corresponding to four different vibration modes respectively.[5]

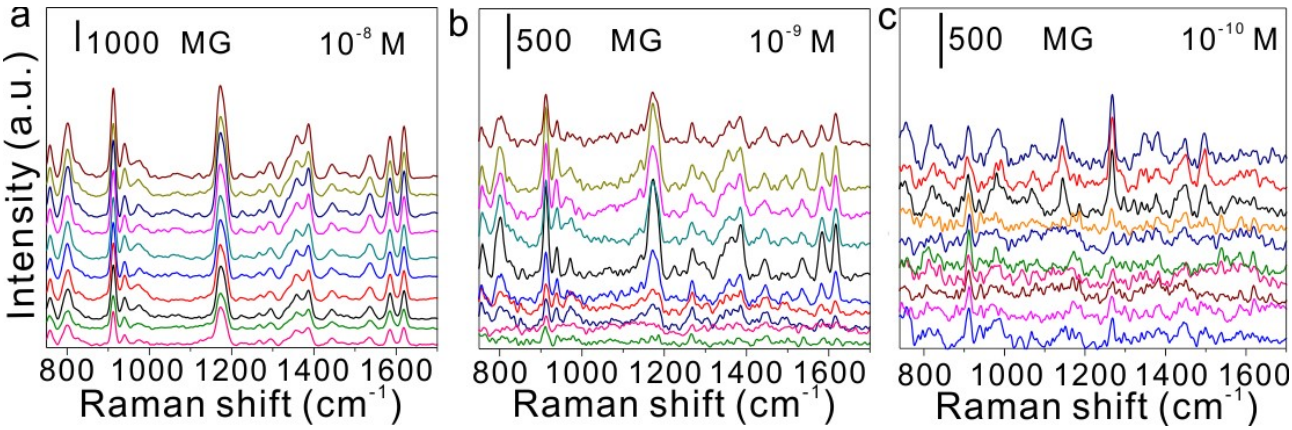

Fig. S10 SERS detection of MG in simulated real environment. SERS spectra of MG on fish surface from 10^{-8} M~10^{-10} M.

MG is a highly toxic, residue-prone, carcinogenic antibiotic. MG has long been listed as a banned drug in aquaculture in China. As Fig. S10 shows, we successfully realized 10^{-10} M MG detection. Characteristic peak 1617 cm^{-1} corresponds to C-C stretching vibration, 800 cm^{-1} corresponds to C-H plane bending vibration, 1367 cm^{-1} and 1390 cm^{-1} correspond to benzene ring stretches and vibrates.[6]

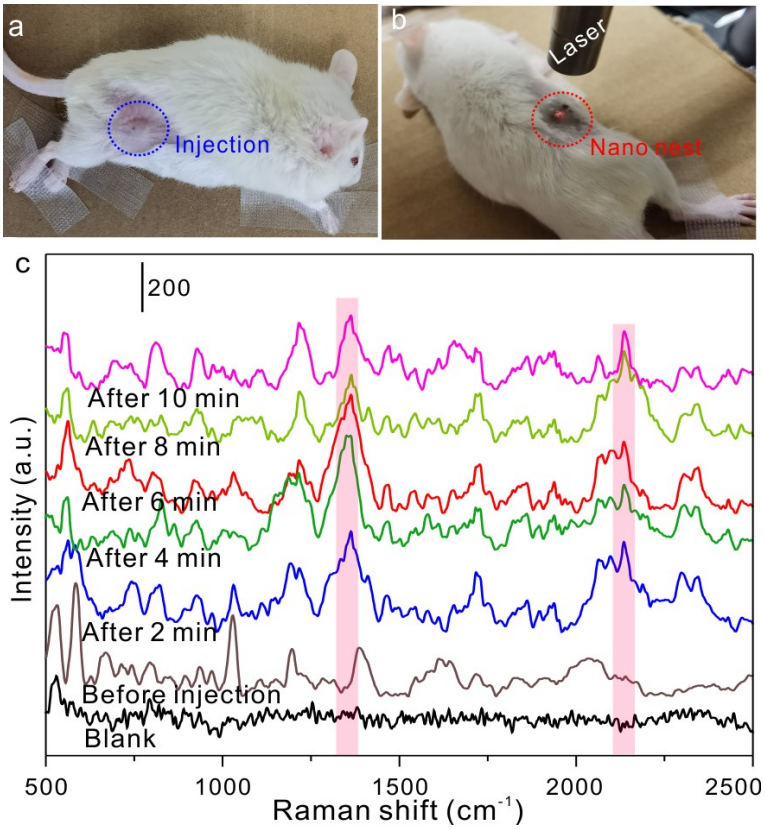

Fig. S11 (a) Image of mouse after subcutaneous injection of formic acid. (b) Image of covered nano nest for SERS in-situ detection. (c) SERS spectra of after injection group within 10 minutes, before injection group and blank (substrate).

As shown in Fig. S11a and S11b, SERS in-situ detection of simulated mosquito bite reaction. After hair removal, injection was performed on the hind leg of the mouse (Fig. S11b). Fig. S11c shows SERS spectra of after injection group within 10 minutes, before injection group and blank (substrate).

References

1. Mitarai, N.; Nori, F., Wet granular materials. *Advances in Physics* **2007,** *55* (1-2), 1-45.

2. Kleinman, S. L.; Ringe, E.; Valley, N.; Wustholz, K. L.; Phillips, E.; Scheidt, K. A.; Schatz, G. C.; Van Duyne, R. P., Single-Molecule Surface-Enhanced Raman Spectroscopy of Crystal Violet Isotopologues: Theory and Experiment. *J Am Chem Soc* **2011,** *133* (11), 4115-4122.

3. Jiang, Q. Y.; Li, D.; Liu, Y. H.; Mao, Z. S.; Yu, Y. J.; Zhu, P.; Xu, Q. L.; Sun, Y.; Hu, L.; Wang, J.; Chen, J.; Chen, F.; Cao, Y., Recyclable and green AuBPs@MoS2@tinfoil box for high throughput SERS tracking of diquat in complex compounds. *Sensor Actuat B-Chem* **2021,** *344*.

4. Wang, C. G.; Wu, X. Z.; Dong, P. T.; Chen, J.; Xiao, R., Hotspots engineering by grafting Au@Ag core-shell nanoparticles on the Au film over slightly etched nanoparticles substrate for on-site paraquat sensing. *Biosensors & Bioelectronics* **2016,** *86*, 944-950.

5. Li, P.; Ge, M. H.; Lin, D. Y.; Yang, L. B., Functionalized acupuncture needle as a SERS-active platform for rapid and sensitive determination of adenosine triphosphate. *Anal Bioanal Chem* **2019,** *411* (22), 5669-5679.

6. Zhou, B. B.; Shen, J. D.; Li, P.; Ge, M. H.; Lin, D. Y.; Li, Y. Y.; Lu, J.; Yang, L. B., Gold Nanoparticle-Decorated Silver Needle for Surface-Enhanced Raman Spectroscopy Screening of Residual Malachite Green in Aquaculture Products. *Acs Appl Nano Mater* **2019,** *2* (5), 2752-2757.